

# **EFFECTS OF SCANDIUM ON HYPO-EUTECTIC ALUMINUM COPPER MICROSTRUCTURES UNDER LOW SOLIDIFICATION RATE CONDITIONS**

A-A. Bogno<sup>1</sup>, J. Valloton<sup>1</sup>, H. Henein<sup>1</sup>, D.G. Ivey<sup>1</sup>, A.J. Locock<sup>2</sup>, M. Gallerneault<sup>3</sup>

<sup>1</sup>Department of Chemical and Materials Engineering, University of Alberta  
Edmonton, Alberta, Canada T6G 1H9

<sup>2</sup>Department of Earth and Atmospheric Sciences, University of Alberta  
Edmonton, Alberta, Canada

<sup>3</sup>Alcereco Inc. Kingston, ON K7L3N6 Canada

Key words: Atomization, Al-alloys, Scandium, Microstructures, Heat treatment

## **Abstract**

This work addresses the microstructures and mechanical properties of Al-4.5 wt% Cu alloys containing 0.1, 0.2 and 0.4 wt% Sc that were solidified under low cooling rate conditions ( $< 1^{\circ}\text{C/s}$ ) and then heat treated. The samples were solidified in a differential scanning calorimeter before being heat treated using two different approaches. The first approach, the traditional sequences of heat treatment, consisted in solutionizing at a constant temperature followed by quenching and aging. The second approach consisted of direct aging of the as-solidified samples. Sc was neither a grain refiner nor a strengthener in the as-solidified conditions. Instead it modified the grain morphology from elongated dendrites to equiaxed structures. While the two heat treatment approaches yielded no significant difference on these slowly solidified Sc containing samples, the resulting mechanical properties are found to be positively affected, provided that much of the Sc is dissolved in the matrix during solidification.

## 1. Introduction

The physical and chemical performance of industrial products obtained from processes such as casting and welding are strongly influenced by their solidification microstructures [1–3]. Variations in solidification conditions, such as the extent of undercooling and/or the cooling rate, and alloy composition are the most efficient ways to control the size and morphology of microstructures. Aluminum alloys are some of the most attractive lightweight materials because of their low densities and high strength-to-weight ratios achievable through cold working and/or heat treatment [4]. The addition of transition metals (TM) such as Cu and Sc to Al results in the formation of finely dispersed precipitates upon heat treatment [5–7]. Such precipitates may result from aging of a supersaturated solid solution promoted by extension of solid solubility during rapid solidification [8], or through solutionizing and quenching the as-cast microstructure at relatively low cooling rates [9]. The Al-Cu system is one of the most widely used base alloys due to the high age-hardening effect of Cu, characterized by the precipitation of finely dispersed Guinier–Preston (GP1 and GP2) zones,  $\theta'$ ,  $\theta''$  and ultimately the stable  $\theta$  phase through heat treatment or even aging at room temperature if the kinetic and thermodynamic conditions in the material are favorable [10,11]. Recently, it has been found that hypereutectic compositions ( $>0.55$  wt% Sc) of Al-Sc based alloys not only promote age hardening through the precipitation of finely dispersed  $\text{Al}_3\text{Sc}$  particles (that can pin grain boundaries and dislocations), but also can provide grain refinement in binary aluminum alloys [12]. Indeed, the grain-refining effect of Sc results from its ability to induce small equiaxed grain formation instead of elongated dendrites, thereby reducing porosity and hot-cracking. Norman et al. [13] showed that hypereutectic ( $>0.55$  wt%) additions of Sc to Al are effective in reducing as-cast grain size from large dendritic grains to fine spherical grains. When combined with other elements, such as Zr, Norman et al. [13] found that the grain refining limit shifted to a lower concentration of Sc. The study of Al-Cu-Sc ternary alloys has been limited to a few experimental investigations [13–17]. Among these, Kharakterova [14] reported that at the Al-rich corner of the ternary phase diagram (Figure 1), depending on the temperature and the nominal Cu and Sc compositions,  $\theta$ - $\text{Al}_2\text{Cu}$  or  $\text{Al}_3\text{Sc}$  and a ternary W-phase may be in equilibrium with primary  $\alpha$ -Al [18,19].

The W-phase has a ThMn<sub>12</sub>-type crystal structure, with unit-cell parameters of  $a = 0.863$  nm and  $c = 0.510$  nm. This corresponds to ScCu<sub>6.6-4</sub>Al<sub>5.4-8</sub> (Al<sub>8+x</sub>Cu<sub>4+x</sub>Sc,  $0 < x < 2.6$ ) [14], which forms over a limited compositional range. As suggested in [16] and corroborated by thermodynamic modelling [17], the W-phase is part of the  $\alpha$ -Al + W and W +  $\theta$ -Al<sub>2</sub>Cu binary eutectics, and takes part in invariant reactions: Liquid (Liq)  $\rightarrow$   $\alpha$ -Al +  $\theta$ -Al<sub>2</sub>Cu + W at 546°C (eutectic) and Liquid (Liq) + Al<sub>3</sub>Sc  $\rightarrow$   $\alpha$ -Al+W at 572°C (peritectic) [17]. In contrast, the Al<sub>3</sub>Sc phase is part of the  $\alpha$ -Al + Al<sub>3</sub>Sc binary eutectic that occurs at 640°C and participates in the four-phase peritectic involving the W-phase at 572°C. Also, it was reported in [13] that Al<sub>3</sub>Sc precipitates first in the melt on crossing the liquidus temperature before the nucleation of  $\alpha$ -Al. The work in [13] suggests that this precipitation sequence is a necessary condition for significant grain refinement to occur. This suggestion was corroborated by the observation of epitaxial growth of  $\alpha$ -Al on primary Al<sub>3</sub>Sc particles.

In order to study the solidification behavior of Al-Cu-Sc and the grain refinement effect of Sc, Norman et al [13] cast hypoeutectic and a hypereutectic compositions of Al-4.5 wt% Cu-0.3 wt% Sc and Al-4.5 wt% Cu-0.8 wt% Sc, respectively, into a wedge-shaped Cu mold to obtain microstructures consisting of fine equiaxed grains at the wedge tip (solidified at about 1000°C/s). Their results showed that significant grain refinement occurred for the alloy with 0.8 wt% Sc (hypereutectic). While only two phases, namely  $\alpha$ -Al and  $\theta$ -Al<sub>2</sub>Cu, were revealed by x-ray diffraction (XRD) analysis of the hypoeutectic composition, additional peaks corresponding to Al<sub>3</sub>Sc were observed for the hypereutectic composition. Al<sub>3</sub>Sc was responsible for refinement of the grain structure. The W-phase was not observed for either alloy composition.

Due to the restricted availability and high cost of Sc, it would be beneficial to minimize the amount of Sc needed to achieve significant grain refinement. Thus, our aim is to study the effect of hypoeutectic Sc compositions (<0.55 wt% Sc) on age-hardenable Al-Cu alloys under various solidification conditions in order to understand the effects of cooling/solidification rates. The objective of this paper, the first of two parts, is to analyze the effect of Sc in the hypoeutectic composition range for Al-4.5 wt% Cu solidified under low solidification rate conditions comparable to processes such as direct chill casting.

## 2. Experiments and methods

### 2.1. Samples production

Al-4.5 wt% Cu and Al-4.5 wt% Cu containing 0.1, 0.2 and 0.4 wt% Sc, in the form of pellets were prepared by alloying 99.99% pure Al with commercial purity Cu and Sc by Novelis. Samples of these alloys were solidified under low cooling rates and low undercooling conditions in a Setaram Labsys Evo 1600 differential scanning calorimeter (DSC) using two alumina crucibles (sample and reference) and a Pt-Rh DSC rod. The DSC furnace was regulated by means of an S-type thermocouple (Pt/Pt-10% Rh), was used to heat the samples in a protective argon atmosphere. A scanning rate of 0.03°C/s to a temperature of 850°C was applied to melt the samples and controlled solidification was achieved by applying a controlled cooling rate. In order to analyze the effect of cooling rate on the solidification path of the investigated alloys, several experiments were carried out under various average cooling rates including 0.01°C/s, 0.08°C/s, 0.3°C/s and 0.8°C/s (maximum cooling rate achievable by the DSC). Temperature was measured directly by thermocouples placed underneath the sample and reference crucibles. Prior to the DSC experiments, the calorimeter was calibrated for temperature and heat measurements using standard samples of Al, Ag, Zn, Sn and Au.

### 2.2. Microstructures characterization techniques

In order to identify the microstructural phases, X-ray diffraction (XRD) analysis was carried out using a Rigaku Geigerflex Powder Diffractometer with incident Co  $K\alpha$  beam with a radiation wavelength of 1.78899 Å. The diffractions were recorded within a wide range of angles ( $2\theta$ ) varying from 5° to 90° with a step of 0.02° and a dwell time of 0.60 s per step. The current and voltage of the X-ray tube were set to 38 mA and 38 kV respectively.

Microstructure examinations were carried out using scanning electron microscopy (SEM) and transmission electron microscopy (TEM), combined with energy dispersive x-ray (EDX)

spectroscopy. SEM of selected samples was carried out with a VEGA3 TESCAN instrument equipped with an EDX analysis system (INCA Microanalysis System, Oxford Instruments). Sample preparation for SEM was achieved by sectioning, grinding and polishing. Backscattered electron (BSE) imaging was utilized to provide atomic number ( $Z$ ) contrast.

TEM was performed with a JEOL 2010 instrument operated at 200 kV and equipped with an ultra-thin window EDX detector. Electron transparent specimens were prepared using focused ion beam (FIB) milling with a Hitachi NB 5000 dual-beam FIB/SEM.

The scale of the microstructure was evaluated by measuring the secondary dendrite arm spacing, approximated by the dendrite cell intervals, i.e. the center-to-center distance between two cells (cell spacing) as visualized on the SEM micrographs. The measurements were carried out using the line intercept method according to ASTM E112-13.

### **2.3. Heat treatment procedures and mechanical properties measurement**

As is common practice in age hardenable Al-Cu alloys and low cooling rate solidification processes such as chill casting, the samples were solutionized for 18.5 h at 535°C in an oven and then quenched in a beaker filled with crushed dry ice before being aged at 240°C for 2 h.

Indeed, the calculated optimum solutionizing temperature and holding time for a hypo-eutectic Al-Cu of similar composition are reported to be 527°C for 10 hours [21]. However, these parameters have not been reported yet for Al-Cu-Sc, therefore, knowing that Sc diffusivity in Al is lower than Cu, the solutionizing temperature was increased to 535°C, about 10°C lower than the melting temperature of the eutectic structure.

The temperature range for aging of hypoeutectic Al-Cu alloys is reported to be 100°C to 250°C [12] and the aging temperature for hypo-eutectic Al-Sc is reported to be 250°C to 350°C [20]. A temperature of 240°C was chosen as it is reported to give the maximum hardening effect on Al-Cu when held for about 2 hours [21]. Aging without solutionizing was also carried out in order to evaluate the amount of Sc still dissolved in the matrix after solidification and to determine how much strengthening can be achieved for slow cooling rates without the usual solutionizing followed by quenching and aging treatments.

Mechanical properties were evaluated through hardness measurements of as-solidified as well as heat treated samples, using a Buehler VH3100 microhardness instrument. The device was

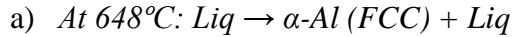
calibrated using a steel block provided by the manufacturer. Five indentations were randomly applied to each sample with a load of 100 gf held for 10 s.

### 3. Results and Discussions

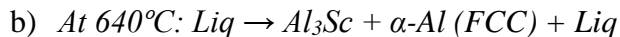
#### 3.1. Effect of Sc on as-solidified Al-4.5 wt% Cu

##### 3.1.1. Gulliver-Scheil prediction

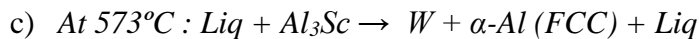
Figure 2 shows sequential solidification of Al-4.5 wt% Cu-0.4 wt% Sc as predicted by Gulliver-Scheil (GS) with the use of the TCAL4 database of Thermo-Calc [19].



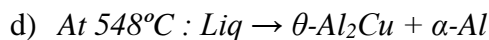
45% of the melt solidifies and grows as primary  $\alpha$ -Al phase in equilibrium with 55% of the liquid remaining when 640°C is reached.



This reaction results in 43% of the remaining 55% melt being transformed into an eutectic  $\alpha$ -Al +  $Al_3Sc$  structure, growing in equilibrium with the already formed  $\alpha$ -Al phase and the remaining 12% melt until 573°C is reached.



This peritectic reaction, consuming about 3% of the remaining 12% melt, leads to the formation of the W-phase at the expense of  $Al_3Sc$ . This results in about 91% of the initial melt being transformed into  $\alpha$ -Al and W-phase forming in equilibrium with the 9% liquid until 548°C is reached.



This eutectic reaction leads to the formation of a binary eutectic structure ( $\alpha$ -Al +  $\theta$ - $Al_2Cu$ ) which forms in equilibrium with the existing  $\alpha$ -Al and W-phase [22].

### 3.1.2. Experimental observations

XRD analysis was carried out on Al-4.5 wt% Cu-0.4 wt% Sc samples solidified at three different cooling rates (0.1, 0.3 and 0.8°C/s). The corresponding diffraction patterns are shown in Figure 3.

The diffraction patterns were indexed to the solid solution phase ( $\alpha$ -Al – major phase) plus three other phases identified as  $\theta$ -Al<sub>2</sub>Cu, Al<sub>3</sub>Sc and Al<sub>8-x</sub>Cu<sub>4+x</sub>Sc, which is in agreement with results published in references [14–17]. However, the diffraction peaks observed for Al<sub>3</sub>Sc were not expected since Al<sub>3</sub>Sc should have been fully consumed during the formation of the W-phase during the peritectic reaction described by the Gulliver-Scheil simulation in Figure 2. Precipitates of Al<sub>3</sub>Sc may have formed during aging at room temperature. In addition, diffraction peaks for AlCu<sub>2</sub>Sc, AlCu<sub>3</sub> and Al<sub>2</sub>O<sub>3</sub> were also detected. Diffraction data for ternary Al<sub>8-x</sub>Cu<sub>4+x</sub>Sc (W-phase) [23] were not found in the ICSD or ICDD-PDF2 databases; therefore, ScFe<sub>4</sub>Al<sub>8</sub> [24] and ThMn<sub>12</sub> [25] whose crystal structures (a= 0.865 nm and c= 0.502 nm and a= 0.863nm and c= 0.496 nm, respectively) are similar to the W-phase [14] were used with JADE 9.0 software to identify the W-phase.

The XRD results corroborate the EDX analysis of the Al-4.5 wt% Cu-0.4 wt% Sc microstructures. Figure 4 shows SEM BSE images of a magnified area around the grain boundaries for solidified Al-4.5 wt% Cu-0.4 wt% Sc, at two different cooling rates. Figure 4a and 4b represent, respectively, the microstructure obtained for a cooling rate of 0.1°C/s and an EDX spectrum of the ternary intermetallic phase. The microstructure consists of the  $\alpha$ -Al phase in equilibrium with blocky Al<sub>2</sub>Cu phases and a compound with elemental composition corresponding to Al<sub>7</sub>Cu<sub>5</sub>Sc. The latter fits quite well with the composition of the W-phase, Al<sub>8-x</sub>Cu<sub>4+x</sub>Sc (0<x<2.6). Figure 4c and 4d are, respectively, the microstructure obtained for a cooling rate of 0.8°C/s and the EDX spectrum from a ternary intermetallic. There are three phases:  $\alpha$ -Al,  $\theta$ -Al<sub>2</sub>Cu and a ternary Al<sub>x</sub>Cu<sub>y</sub>Sc<sub>z</sub> phase. The ternary phase, which is finer than the one in the microstructure obtained at 0.1°C/s, could not be identified as the W-phase or any known ternary phase. Because of the relatively small size of the ternary precipitates, i.e., they are less than the size of the X-ray interaction volume, the actual composition could not be determined. TEM analysis, which has a much smaller interaction volume for X-ray microanalysis and diffraction capability, was required to identify these precipitates.

A FIB specimen was prepared for the Al-4.5 wt% Cu-0.4 wt% Sc sample cooled at 0.8°C/s, from a region containing the unknown ternary phase along the grain boundary of the  $\alpha$ -Al phase. Figure 5a shows a TEM bright field (BF) image of this sample. In Figure 5b, a selected area diffraction (SAD) pattern of the matrix phase (spot 1) has been indexed to  $\alpha$ -Al. Figure 5d shows an EDX spectrum from the  $\alpha$ -Al phase, showing that it consists of Al and some dissolved Cu. An SAD pattern from the precipitate (spot 2) can be indexed to the structure of the W-phase (Figure 5c), i.e.,  $\text{Al}_{8-x}\text{Cu}_{4+x}\text{Sc}$ .  $\text{Al}_{8-x}\text{Cu}_{4+x}\text{Sc}$  has a tetragonal crystal structure; the lattice parameters were calculated as  $a = 0.855$  nm and  $c = 0.505$  nm, which are close to those of  $\text{ScFe}_4\text{Al}_8$  [24] and  $\text{ThMn}_{12}$  [25] with similar structures as the W-phase and also close to the values ( $a = 0.863$  nm and  $c = 0.510$  nm) reported in the literature [14]. Figure 5e shows an EDX spectrum from the W-phase. Several precipitates detected through XRD analysis, i.e.,  $\text{AlCu}_2\text{Sc}$ ,  $\text{AlCu}_3$  and  $\text{Al}_2\text{O}_3$ , were not identified within the investigated microstructures. The XRD peaks for  $\text{AlCu}_2\text{Sc}$  and  $\text{AlCu}_3$  were quite weak and only 2 or 3 peaks were identified. As such, their identification is not conclusive and even if they were present in the solidified alloys, they could have been missed during microstructure analysis. The presence of  $\text{Al}_2\text{O}_3$  is more certain as several peaks with significant intensities were identified in the XRD patterns.

The Al-4.5 wt% Cu-0.4 wt% Sc samples used for XRD and SEM analysis were solidified at the same cooling rates, but were taken from different runs. Thus, the precipitation of  $\text{Al}_2\text{O}_3$  may have been promoted by residual oxygen in the solidification chamber (the oxygen content was not measured during these experiments), despite purging the chamber with argon. The  $\text{AlCu}_2\text{Sc}$  and  $\text{AlCu}_3$  peaks (small amounts) present in the XRD patterns are likely due to non-equilibrium precipitation of these phases. The microstructures for both cooling rates show no evidence of  $\text{Al}_3\text{Sc}$ , probably because the amount was too small and may not have been present in regions imaged. It is worth noting that the ternary W-phase observed for both cooling rates seems to have grown on the  $\theta$ - $\text{Al}_2\text{Cu}$  phase in a divorced eutectic configuration. Its size seems to decrease as the cooling rate is increased. Also, the observed  $\theta$ - $\text{Al}_2\text{Cu}$  phase has a completely blocky morphology for the lower cooling rate of 0.1°C/s and a partially blocky and partially eutectic morphology for the higher cooling rate (0.8°C/s). This is in agreement with the results found in [26], where the  $\text{Al}_2\text{Cu}$  morphology is attributed to the cooling rate and the level of modification of that phase.

### 3.1.3. Experimental transformation temperatures

The DSC tests resulted in curves representing the variation in heat flux with temperature. The transition enthalpies corresponding to the areas under the DSC curves were calculated for each transformation. Two cooling rates, 0.8°C/s and 0.1°C/s were chosen to describe the phase transformations during solidification of the investigated samples. Solidification at 0.1°C/s was chosen because it is the cooling rate at/below which the DSC cooling curves for Al-4.5 wt% Cu-0.4 wt% Sc show evidence of three exothermic peaks. Above 0.1°C/s only two exothermic peaks are observed for all investigated alloy compositions.

Figure 6a shows the DSC cooling curve for Al-4.5 wt%-0.4 wt% Sc solidified at 0.1°C/s. Three exothermic peaks can be identified at onset temperatures of 654°C, 560°C and 552°C. The DSC cooling curve for the same alloy composition, but cooled at 0.8°C/s (Figure 6b), has only two peaks with onset temperatures of 651°C and 542°C. An onset temperature is defined as the intersection between the tangent to the maximum rising slope of a peak and the extrapolated sample baseline. For Al-4.5 wt% Cu without Sc addition, solidified under identical conditions, two peaks are present (Figure 6c) with onset temperatures of 642°C and 542°C. For Al-4.5wt% Cu, these two peaks certainly correspond to the formation of primary  $\alpha$ -Al phase and the eutectic structure ( $\alpha$ -Al +  $\theta$ -Al<sub>2</sub>Cu), respectively.

While the transition temperatures corresponding to the first transformation appear to be slightly different, the temperature corresponding to the second transformation is the same for both the binary Al-4.5 wt% Cu alloy and the Al-4.5 wt% Cu alloy with 0.4 wt% Sc, cooled at 0.8°C/s. However, Figure 7 reveals a small exothermic peak at around 542°C, which was obtained by subtracting the cooling curve for the Al-4.5 wt% Cu alloy from the one corresponding to Al-4.5 wt% Cu-4 wt% Sc, both solidified at 0.8°C/s.

Figure 8 shows the variation in transition temperatures with cooling rate for each investigated alloy. Extrapolation to equilibrium solidification (0°C/min) is indicated by arrows on each figure. For each investigated alloy, there are two types of transformations, i.e., the precipitation of the primary phase ( $\alpha$ -Al) followed by the eutectic transformation, except for the alloy with the highest Sc content (0.4 wt % - Figure 8d).

For the 0.4 wt% Sc alloy (Figure 8d), a third peak is observed at a transition temperature of 573°C when the cooling rate is 0.1°C/s and lower, which may correspond to the peritectic reaction  $L + Al_3Sc \rightarrow \alpha-Al + W + L$  [14] before the eutectic reaction  $L \rightarrow \alpha-Al + \theta-Al_2Cu + W$  at 554°C. This

is in agreement with the results published in [14–17] and with Gulliver-Scheil (GS) solidification predictions obtained through the TCAL4 database of Thermo-Calc [19] as shown in Figure 2.

It is worth noting that the experimental transition temperatures decrease with increasing cooling rate for all four compositions. This trend is expected as nucleation undercooling generally increases with cooling rate [27, 28].

The equilibrium transition temperatures obtained by extrapolation are plotted against the concentration of Sc for each investigated alloy in Figure 9. There is a slight increase in the nucleation temperature as the Sc level is increased, suggesting that Sc promotes early nucleation and, therefore, lowers the amount of nucleation undercooling in agreement with the results obtained in [29].

These results suggest that for Al-4.5 wt% Cu-0.4 wt% Sc solidified at 0.8°C/s, two different phase transformations occur, i.e.,  $L \rightarrow \alpha + L$  at 651°C and a eutectic reaction  $L \rightarrow \alpha + \theta + W$  at 542°C. At a lower cooling rate of 0.1°C/s, three different phase transformations occur, i.e.,  $L \rightarrow \alpha + L$  at 654°C, a peritectic reaction  $L + Al_3Sc \rightarrow \alpha + W + L$  at 560°C and finally a eutectic reaction  $L \rightarrow \alpha + \theta$  at 552.4°C. The peritectic reaction suggests that there was prior precipitation of  $Al_3Sc$  (as detected by XRD), but the corresponding peak was not observed on the DSC curve. This peak may be relatively small and may have been obscured by the larger peak corresponding to  $\alpha$ -Al precipitation.

#### **3.1.4. Scale of microstructures and mechanical properties**

Figure 10 shows SEM BSE images of typical microstructures corresponding to the four investigated alloy compositions solidified at 0.8°C/s. The microstructure varies from dendritic to equiaxed cells as the Sc concentration increases from 0.0 wt% to 0.4 wt%.

The corresponding secondary dendrite arm spacing (SDAS)/cell spacing for each composition is shown in Figure 11. For the same cooling rate, the microstructural scale is similar for Sc content up to 0.2 wt%. However, as the microstructural morphology changes from long dendritic to equiaxed grains at 0.4 wt% Sc level, the microstructure becomes coarser. As such, SDAS are measured for Sc levels up to 0.2 wt%, while grain size/cell spacing is measured for alloys with 0.4 wt% Sc.

Mechanical properties were evaluated via Vickers microhardness measurements. Hardness (VH) variation as a function of Sc content is negligible (Figure 11), suggesting that the addition of Sc to the hypoeutectic Al-Cu alloy is not an effective strengthener during low cooling rate solidification processes. It is worth noting that, although the microstructure is coarser for higher levels of Sc (0.4 wt %) compared with lower levels of Sc additions, all the samples show similar microhardness values. This result demonstrates that hardness is not a function of cell spacing only, but depends also on phase composition (solid solution).

### **3.2. Effect of Scandium on heat treated Al-4.5 wt% Cu**

The effect of Sc on heat treated Al-4.5 wt% Cu was evaluated through Vickers microhardness tests. Two different heat treatment processes were conducted on the as-solidified (50°C/s) samples. The first heat treatment consisted in aging the samples at 300°C for 20 hours. The second one consisted in solutionizing the samples at 535°C for 18.5 hours before transferring them into a beaker filled with dry ice for quenching and then aging them at 240°C for 2 hours. It is worth mentioning that, there was no liquid (e.g., acetone or ethanol) mixed with the crushed dry ice, however, the samples were fully immersed into the ice. Although, there was no direct control over the cooling rate, the samples must have cooled rapidly enough under these conditions. Indeed, a water bath at 80°C is often used as a quenching agent for castings [30]; therefore, the cooling rate in this work should be high enough to be compared with industrial procedures. Moreover, as will be shown later, the as-quenched Al-4.5 wt% Cu sample did not show any evidence of precipitation (at the micron scale).

Figure 12 shows the microhardness results for both heat treatments conditions as well as for the as-solidified condition for comparison. After aging the samples at 300°C for 20 h, the hardness increases with increasing Sc content. However, at low levels of Sc (<0.1 wt% Sc), hardness of aged samples is lower than the hardness of the as-solidified samples. The hardness is expected to be affected by two factors. One is that any Sc still in solid solution will come out as Al<sub>3</sub>Sc precipitates and harden the alloy, which explains the hardness increase with Sc content. In addition, grain growth can occur at 300°C, which has the effect of decreasing hardness. For the samples that contain low levels of Sc (<0.1 wt% Sc) and have been solidified at 0.8°C/s (low cooling rate), there is only limited precipitation of Sc from the  $\alpha$ -Al matrix to form Al<sub>3</sub>Sc and the

hardening effect is more than offset by grain growth resulting in a lower hardness. For higher levels of Sc addition ( $>0.1$  wt %), there is more Sc dissolved in the primary phase which counters the effect of grain growth. Hence, there is a small hardness increase compared the corresponding as-solidified samples. After solutionizing at  $535^{\circ}\text{C}$  for 18.5 h, quenching and then aging at  $240^{\circ}\text{C}$  for 2h, all the samples (all Sc levels) are harder than the corresponding as-solidified ones. Solutionizing led to the dissolution of all the intermetallics (Figure 13a) for samples with Sc level  $<0.1$ wt%, so that upon subsequent aging, nucleation of finely dispersed  $\text{Al}_2\text{Cu}$  precipitates are expected [31] . For samples with higher Sc levels ( $>0.1$  wt %), dissolution of the intermetallics is not complete after solutionizing, as Sc- and Cu-rich phases are still present at the grain boundaries (Figure 13b). it is therefore assumed that there would be lesser amount of solute dissolved in the matrix during solutionizing as compared to the samples with lower Sc levels, in which full dissolution of the grain boundaries are observed. Consequently, for samples with incomplete dissolution of the grain boundaries, a lower amount of  $\text{Al}_2\text{Cu}$  precipitates from the solid solution is expected during aging [31], which may have led to the lower microhardness values observed for samples with Sc  $>0.1$  wt% as compared with samples containing lower Sc levels.

#### 4. Conclusions

Al-4.5 wt% Cu alloys with different Sc additions (0.1 wt%, 0.2 wt% and 0.4 wt %) were solidified by differential scanning calorimetry. Samples with different thermal histories were generated by varying the cooling rate from  $0.1^{\circ}\text{C}/\text{s}$  to  $0.8^{\circ}\text{C}/\text{min}$ . The effects of cooling rate and Sc level on the microstructure scale, phase formation and mechanical properties were analysed. The following conclusions can be drawn from the analyses:

1. Two phases are in equilibrium with  $\alpha$ -Al: binary  $\theta$ - $\text{Al}_2\text{Cu}$  and a ternary  $\text{Al}_{8-x}\text{-Cu}_{4+x}\text{-Sc}$  W-phase.
2. The size of the W-phase precipitates decreases with increasing cooling rate.
3. The addition of Sc does not refine the microstructure within the investigated cooling rates; instead Sc modifies the grain morphologies from long dendritic to equiaxed.
4. The addition of Sc does not strengthen the as-solidified alloys and after age hardening the strengthening effect is still negligible.

5. The addition of Sc to hypo-eutectic Al-Cu alloys is not effective as an age hardener strengthener under low solidification rate conditions. Much of the Sc is tied up with Cu in the form of the intermetallic W-phase. For the conditions studied (low cooling rates), there appears to be no benefit to adding Sc, in the hypoeutectic composition, to Al-4.5 wt% Cu if the traditional heat treatment route is followed. However, a minor improvement in hardness is observed upon ageing immediately after solidification when 0.4 wt% Sc is added.

### **Acknowledgements**

The authors are grateful to Thermo-Calc and Paul Mason for providing the Scheil solidification diagram. Thanks are also due to Kai Cui for the TEM sample preparation using FIB at the National Institute for Nanotechnology (NINT, Edmonton, AB, Canada). Finally, the Natural Sciences and Engineering Research Council (NSERC) of Canada is gratefully acknowledged for their financial support.

## References

- [1] S.A. David, J.M. Vitek, Correlation between solidification parameters and weld microstructures. *Int. Mat. Rev.* (1989); 34: 213.
- [2] S.A. David, S.S. Babu, J.M. Vitek, Welding: Solidification and microstructure. *JOM* (2003); 55: 14.
- [3] W.J. Boettinger, S.R. Coriell, A.L. Greer, et al. Solidification microstructures: recent developments, future directions. *Acta Mater.* (2000); 48: 43.
- [4] I.N. Fridlyander, V.G. Sister, O.E. Grushko, et al. Aluminum alloys: promising materials in the automotive industry. *Metal. Sci. Heat Treat.* (2002); 44: 365.
- [5] I. Polmear. *Aluminium Alloys - A Century of Age Hardening*. Proceedings of the 9<sup>th</sup> International Conference on Aluminium Alloys. (2004); 28:1.
- [6] R.S. Rana, R. Purohit, S. Das. Reviews on the influences of alloying elements on the microstructure and mechanical properties of aluminum alloys and aluminum alloy composites. *Int. J. Sci. Res. Publ.*(2012); 2:1.
- [7] D.S. MacKenzie. Heat treatment of aluminum alloys. *Ind. Heat.* (2004); 71(12):29.
- [8] E. Lavernia, T. Srivatsan. The rapid solidification processing of materials: science, principles, technology, advances, and applications. *J. Mater. Sci.* (2010); 45:287.
- [9] D. Emadi, A.K.P. Rao, M. Mahfoud. Influence of scandium on the microstructure and mechanical properties of A319 alloy. *Mater. Sci. Eng. A.* (2010); 527: 6123.
- [10] M.J. Starink, N. Gao, J.L. Yan, The origins of room temperature hardening of Al-Cu-Mg alloys. *Mater. Sci. Eng. A.* (2004); 387–389 (1–2 special issue): 222.
- [11] A. Cochard, K. Zhu, S. Joulié, et al. Natural aging on Al-Cu-Mg structural hardening alloys – investigation of two historical duralumins for aeronautics. *Mater. Sci. Eng. A.* (2017); 690: 259.
- [12] J. Røyset. Scandium in aluminium alloys overview: Physical metallurgy, properties and applications. *Metall. Sci. Tech.* (2007); 25: 11.
- [13] A. Norman, P. Prangnell, R. McEwen. The solidification behaviour of dilute aluminium-scandium alloys. *Acta Mater.* (1998); 46: 5715.
- [14] M.L. Kharakterova. Phase composition of Al-Cu-Sc alloys at temperatures at 450 and 500 deg C. *Izv. Akad. Nauk SSSR Met.* (1991); 4: 191.
- [15] M.L. Kharakterova, D.G. Eskin, L.S. Toropova. Precipitation hardening in ternary alloys of the Al-Sc-Cu and Al-Sc-Si systems. *Acta Met. Mat.* (1994); 42: 2285.
- [16] L.S. Toropova, D.G. Eskin, M.L. Kharakterova, et al. *Advanced Aluminum Alloys Containing Scandium, Structure and Properties*. Gordon and Breach Science Publishers.

- (1998).
- [17] H. Bo, L.B. Liu, Z.P. Jin. Thermodynamic analysis of Al–Sc, Cu–Sc and Al–Cu–Sc system. *J. Alloys Compd.* (2010); 490: 318.
  - [18] J.O. Andersson, T. Helander, L. Höglund, et al. Thermo-Calc and DICTRA, computational tools for materials science, *Calphad.* (2002); 26: 273.
  - [19] Thermo-Calc Database, TCAL4. (2008).
  - [20] J. Røyset, N. Ryum, D. Bettella, et al. On the addition of precipitation- and work-hardening in an Al–Sc alloy. *Mat. Sci. Eng. A.* (2008); 483: 175.
  - [21] C.-A. Gandin, Y. Bréchet, M. Rappaz, et al. Modelling of solidification and heat treatment for the prediction of yield stress of cast alloys. *Acta Mater.* (2002); 50: 901.
  - [22] P. Riani, L. Arrighi, R. Marazza, et al. Ternary rare-earth aluminum systems with copper: a review and a contribution to their assessment. *J. Phase Equil. Diff.* (2004); 25: 22.
  - [23] W. Suski, T. Cichorek, K. Wochowski, et al. Low-temperature electrical resistance of the U(Cu,Ni)<sub>4</sub>Al<sub>8</sub> system and magnetic and electrical properties of ScCu<sub>4+x</sub>Al<sub>8-x</sub>. *Phys. B.* (1997); (230–232): 324.
  - [24] B.Y. Kotur, D. Badurski, W. Suski, et al. Structure, magnetic and electrical properties of ScFe<sub>x</sub>Al<sub>1-x</sub> alloys and their relation to the UFe<sub>x</sub>Al<sub>1-x</sub> system. *Phys. B.* (1998); 254: 107.
  - [25] H. Misiorek, J. Stępień-Damm, W. Suski, et al. Lattice parameters, magnetic susceptibility and thermal conductivity of ScFe<sub>4</sub>Al<sub>8</sub> and YFe<sub>4</sub>Al<sub>8</sub>. *J. Alloys Compd.* (2004); 36: 381.
  - [26] L.J. Colley, M.A. Wells, R. MacKay, et al. Dissolution of second phase particles in 319-type aluminium alloy. *Heat Treating 2011: Proceedings of the 26th Conference.* ASM International. (2011); 189.
  - [27] B. Yang, Y. Gao, C. Zou, et al. Cooling rate dependence of undercooling of pure Sn single drop by fast scanning calorimetry. *Appl. Phys. A Mater. Sci. Process.* (2011); 104: 189.
  - [28] Y.L. Gao, E. Zhuravlev, C.D. Zou, et al. Calorimetric measurements of undercooling in single micron sized SnAgCu particles in a wide range of cooling rates. *Thermochim. Acta.* (2009); 482: 1.
  - [29] A.-A. Bogno, J. Valloton, P. Natzke, et al. Scandium effects on nucleation undercooling in Al-Cu droplets generated by impulse atomization and electro-magnetic levitation. *Materials Science and Technology Conference and Exhibition.* 2015; 2.
  - [30] A. K. Dahle. Aluminum Alloys, Heat Treatment of. in *Encyclopedia of Materials: Science and Technology.* (2001); 111.
  - [31] M. Jia, Z. Zheng, and Z. Gong. Microstructure evolution of the 1469 Al-Cu-Li-Sc alloy during homogenization. *J. Alloys Compd.* (2014); 614: 131.

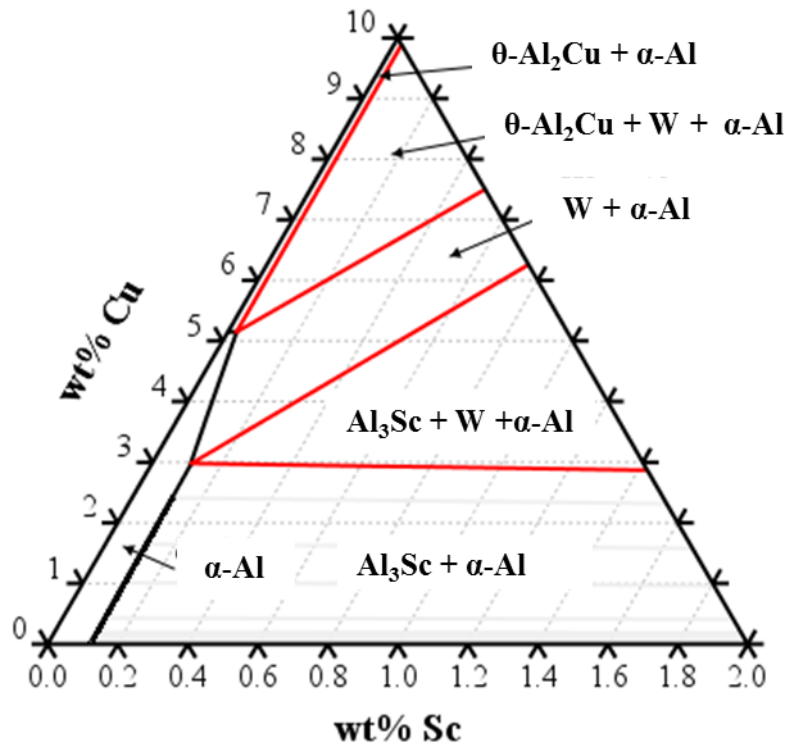


Figure 1: Isothermal section of the Al-rich corner of the Al-Cu-Sc system at 535°C [19].

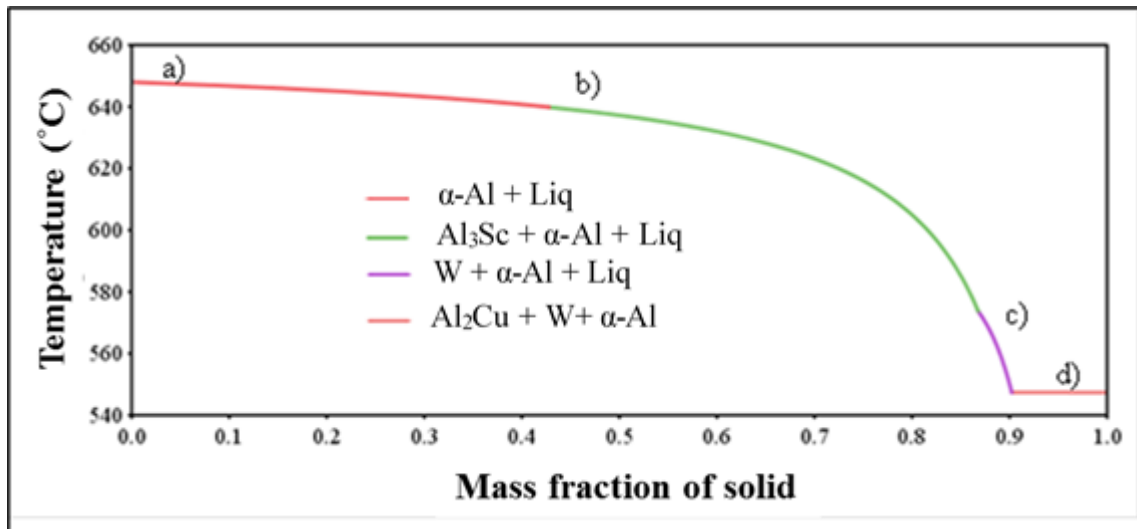


Figure 2: Gulliver-Scheil prediction of phase formation during solidification of Al-4.5 wt% Cu-0.4 wt% Sc alloy, obtained through the TCAL4 database of Thermo-Calc [19].

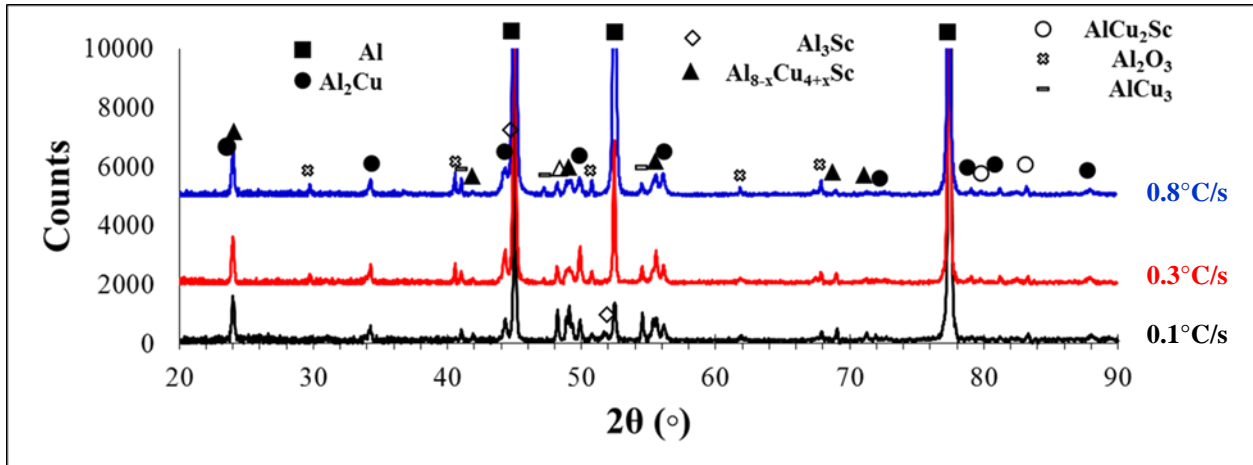


Figure 3: XRD patterns after DSC solidification of Al-4.5 wt% Cu-0.4 wt% Sc alloys at 3 different cooling rates.

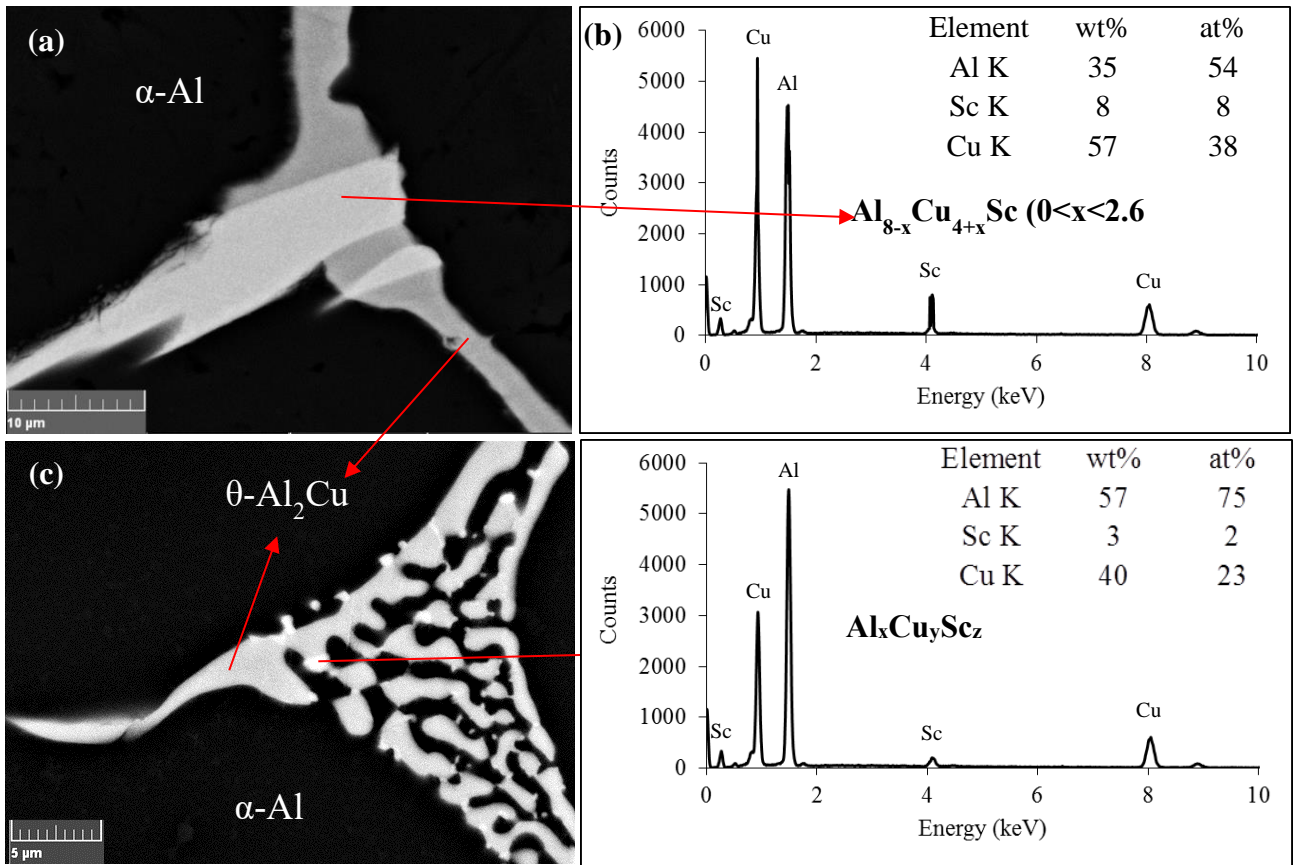


Figure 4: Microstructure analysis for Al-4.5 wt% Cu-0.4 wt% Sc alloy: (a) SEM BSE image of primary  $\alpha$ -Al phase and the eutectic structure for a cooling rate of 0.1 °C/s. (b) EDX spectrum from the Al-Cu-Sc ternary phase precipitate. (c) SEM BSE image of primary  $\alpha$ -Al phase and intermetallic for a cooling rate of 0.8 °C/s. (d) EDX spectrum from intermetallic phase in the interdendritic region.

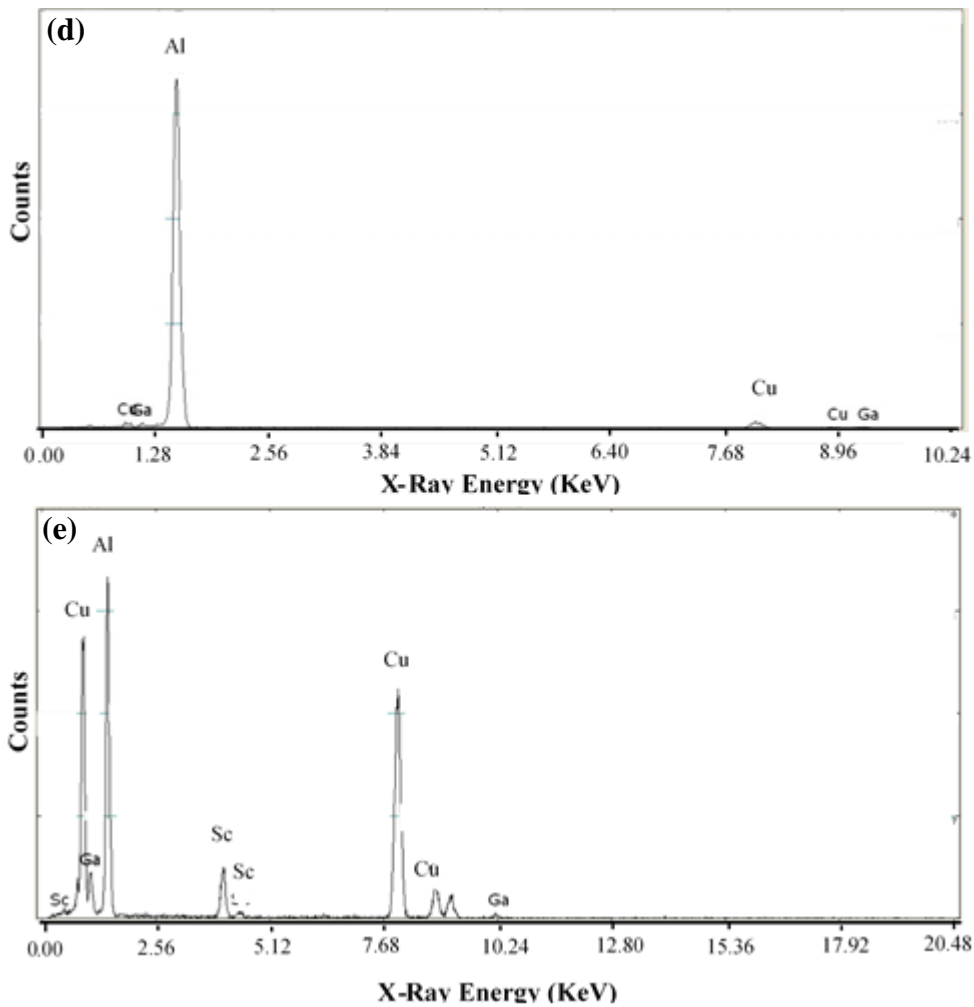
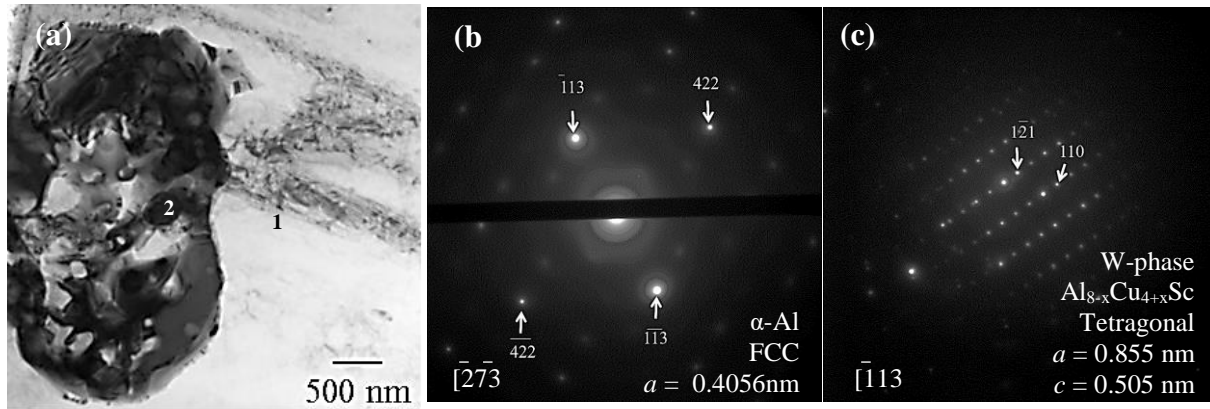


Figure 5: (a) TEM BF image of Al-4.5 wt% Cu-0.4 wt% Sc sample cooled at 0.8°C/s. (b) SAD pattern of the spot marked as 1 in (a); the zone axis is along  $[\bar{2}7\bar{3}]$  for  $\alpha$ -Al. (c) SAD pattern of the spot marked as 2 in (a); the zone axis is  $[\bar{2}13]$  for the W-phase. (d) EDX spectrum from the spot marked as 1 in (a). (e) EDX spectrum from the spot marked as 2 in (a). The Ga peaks in the EDX spectra are artifacts of FIB sample preparation.

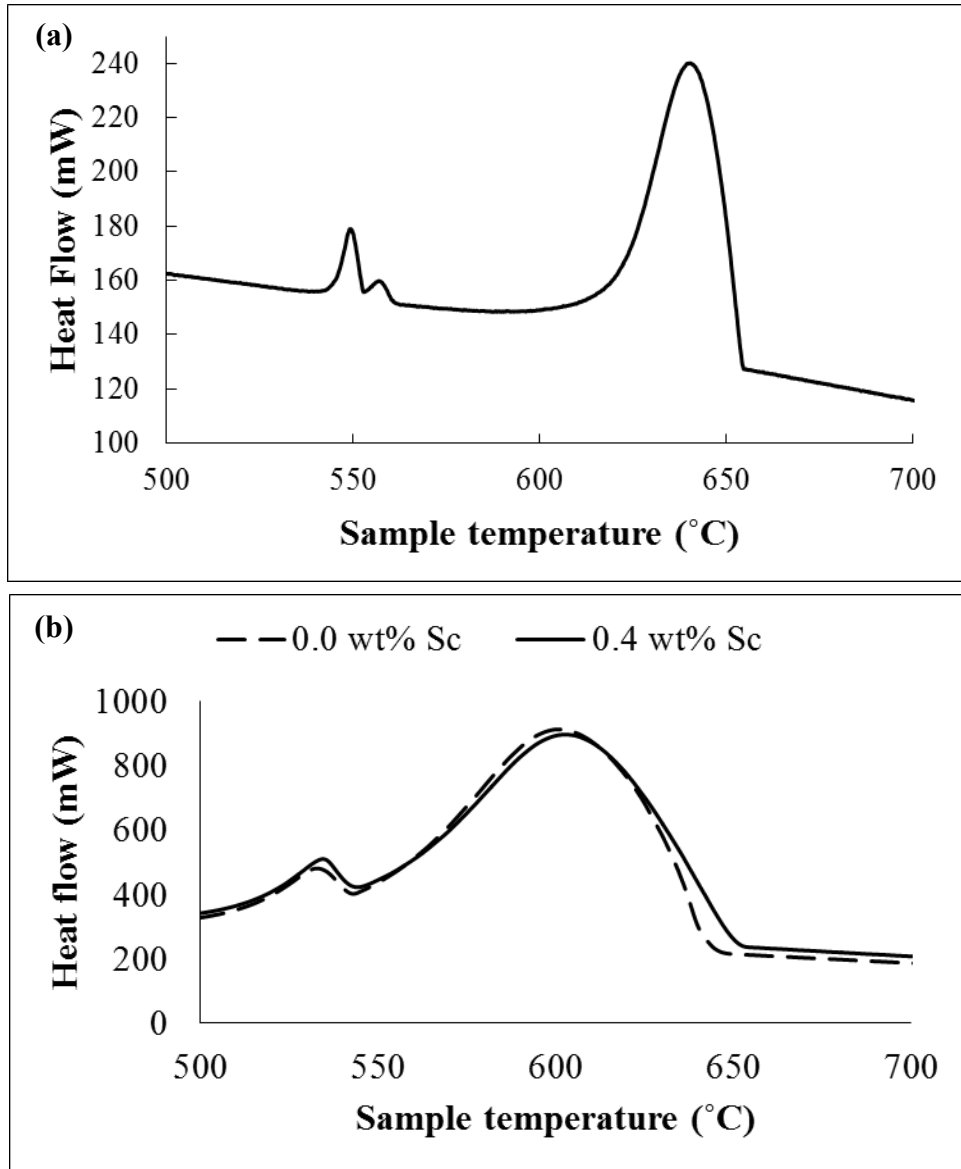


Figure 6: DSC solidification curves (a) Al-4.5 wt% Cu-0.4 wt% Sc cooled at 0.1 °C/s and (b) Al-4.5 wt% Cu-X Sc (X=0.0wt% and X=0.4wt%) cooled at 0.8 °C/s.

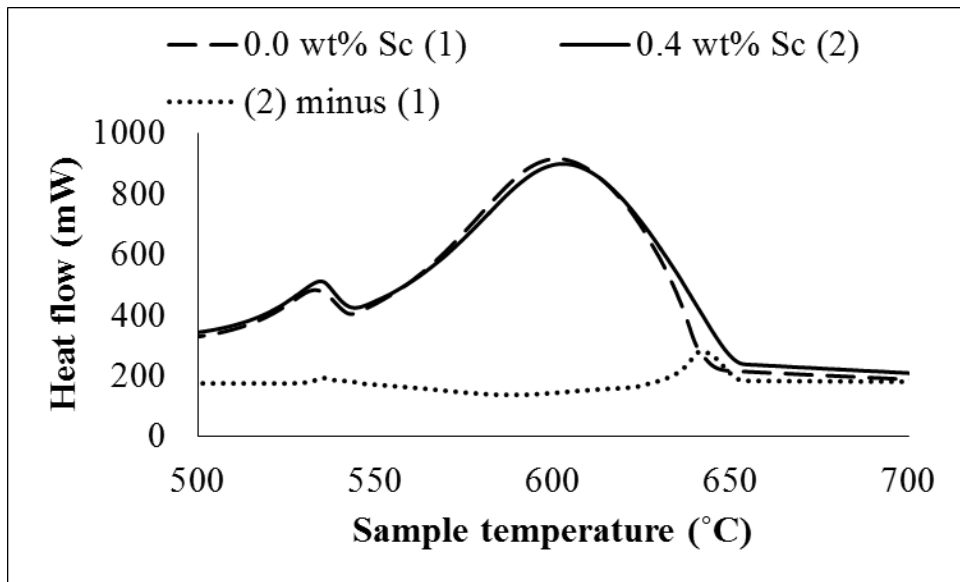


Figure 7: DSC solidification curves for Al-4.5 wt% Cu and Al-4.5 wt% Cu-0.4 wt% Sc alloys, both cooled at 0.8°C/s. The dotted curve is the result after subtracting the first curve from the second.

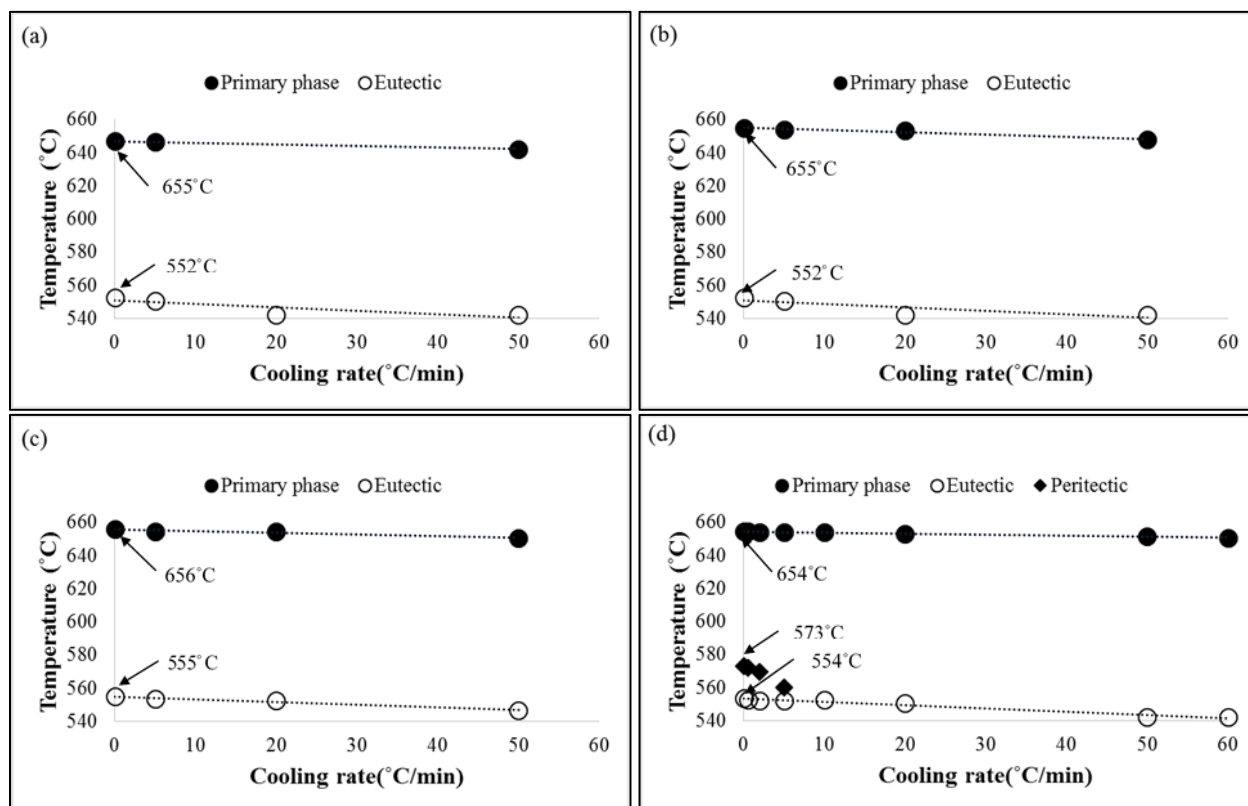


Figure 8: Variation in transition temperatures with cooling rate for the four investigated Al-4.5 wt% Cu alloys with different levels of Sc: (a) 0.0 wt% Sc, (b) 0.1 wt% Sc, (c) 0.2 wt% Sc and (d) 0.4 wt% Sc. Arrows indicate the extrapolated transition temperatures at 0°C/s.

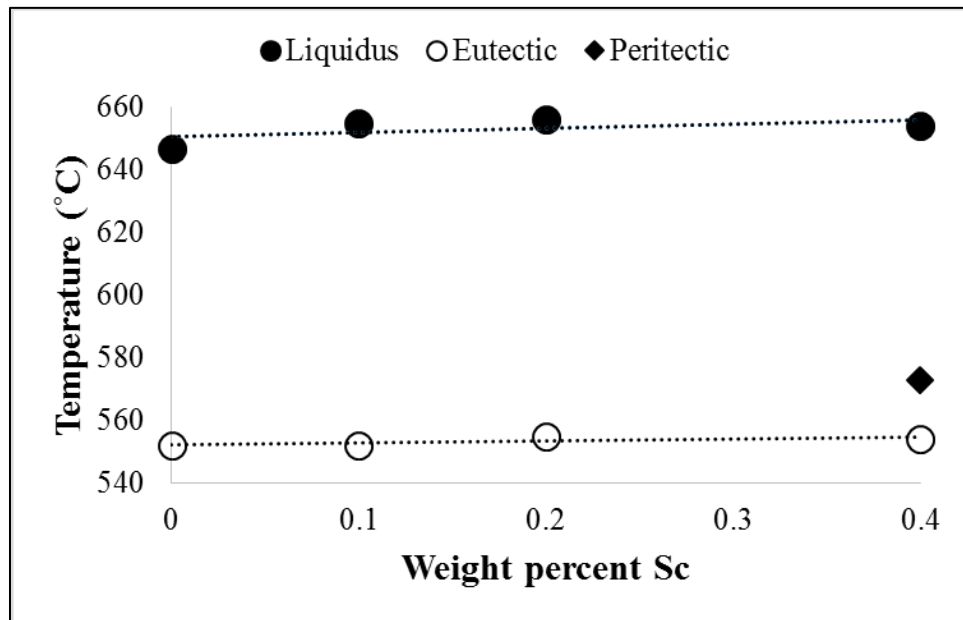


Figure 9. Variation of equilibrium transition temperature as a function of Sc content in Al-4.5 wt% Cu.

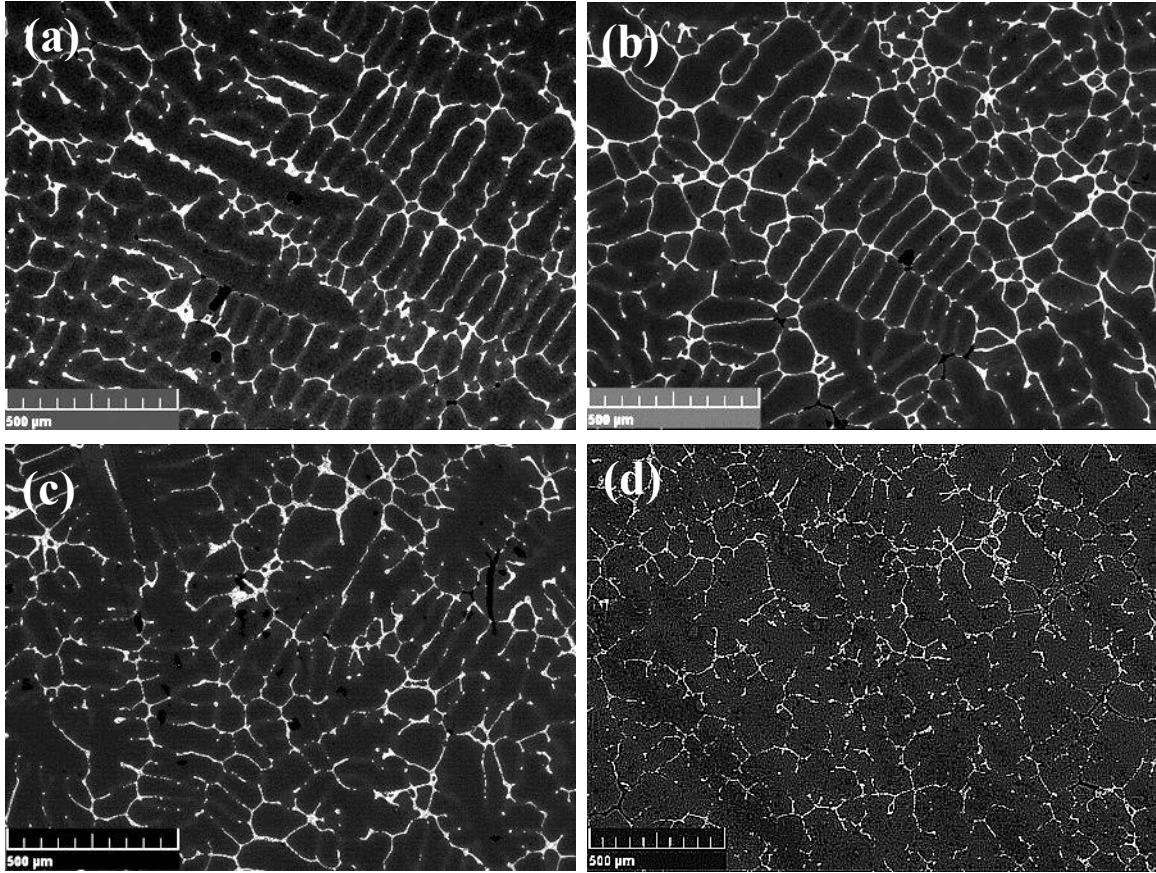


Figure 10: Representative solidification microstructures of investigated Al-4.5 wt% Cu alloys with different Sc additions cooled at the 0.8°C/s: (a) 0.0 wt% Sc, (b) 0.1 wt% Sc, (c) 0.2 wt% Sc and (d) 0.4 wt% Sc.

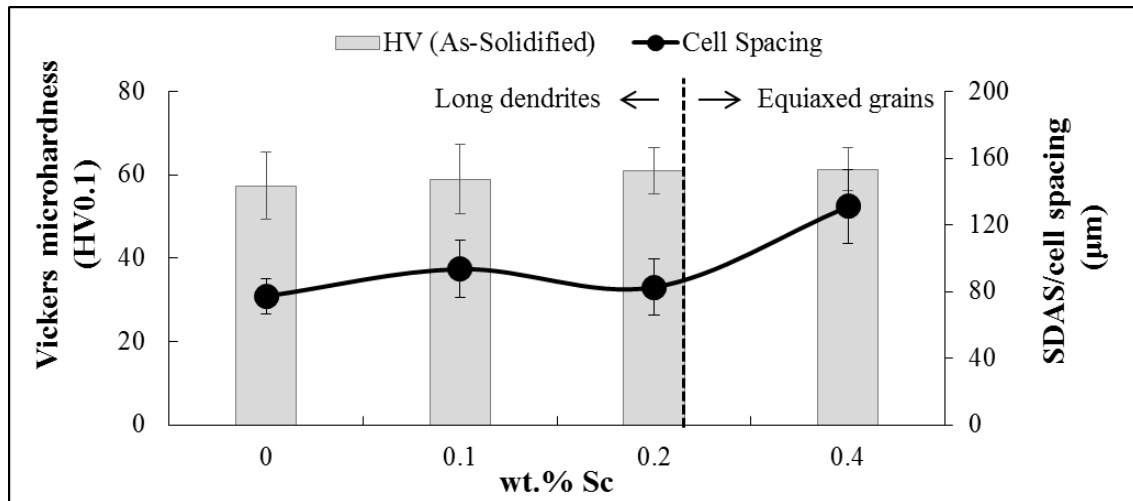
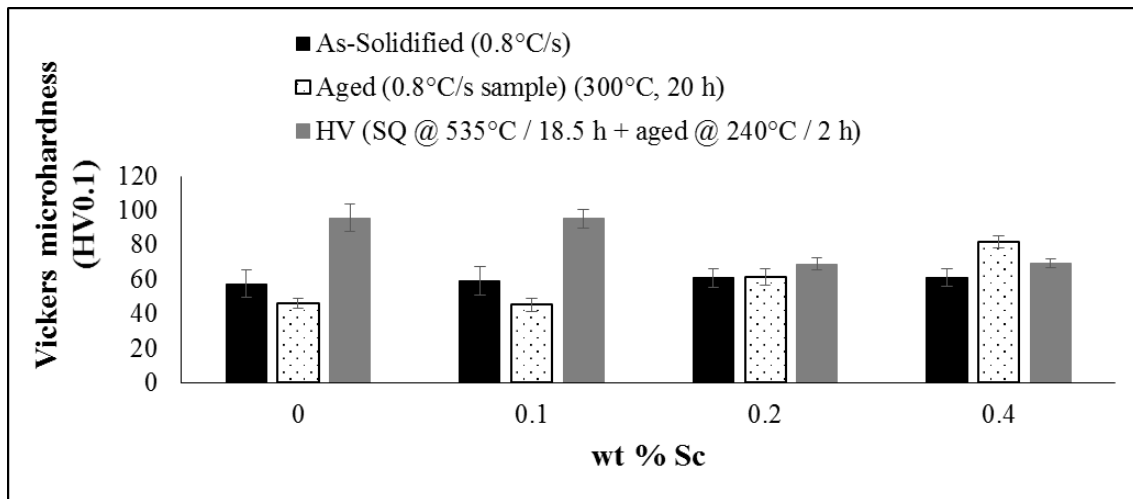
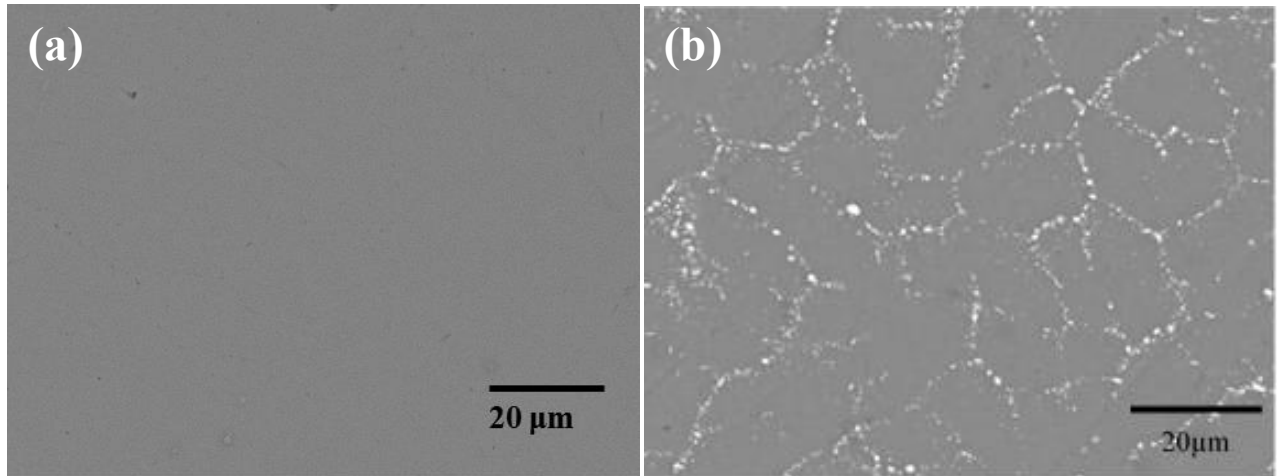


Figure 11: Variation of cell spacing and Vickers microhardness with Sc nominal composition in Al-4.5 wt% Cu alloy solidified at 0.8°C/s.



*Figure 12: Variation in Vickers microhardness with Sc concentration in Al-4.5 wt% Cu (Sc) alloys after solutionizing at 535°C for 18.5 hours and quenching in a beaker filled with crushed dry ice before aging at 240°C for 2 hours.*



*Figure 13: Al-4.5 wt% Cu with different Sc additions solutionized for 535°C for 18.5 hours and quenched with dry ice. (a) 0.0 wt% Sc and (b) 0.4 wt% Sc.*